# Protein-Resistant NTA-Functionalized Polymer Brushes for Selective and Stable Immobilization of Histidine-Tagged Proteins

**Julien E. Gautrot,*,† Wilhelm T. S. Huck,† Martin Welch,‡ and Madeleine Ramstedt*,†,§**

Melville Laboratory for Polymer Synthesis, Department of Chemistry, University of Cambridge, Lensfield Road, Cambridge CB2 1EW, U.K., Department of Biochemistry, University of Cambridge, Hopkins Building, Downing Site, Cambridge CB2 1QW, U.K., and Department of Chemistry, Umeå University, SE-90187 Umeå, Sweden

**ABSTRACT** Protein-resistant polymeric coatings that allow highly selective immobilization of specific biomolecules are essential for biomedical applications such as microarrays, biosensing, heterogeneous catalysis, and bioengineering. Polymer brushes are particularly interesting for this purpose because their chemical structure and physical properties can easily be tailored to meet specific needs. This article explores the functionalization of two protein-resistant polymer brushes, poly(oligoethylene glycol methacrylate) (POEGMA) and poly(hydroxyethyl methacrylate) (PHEMA), with nitrilotriacetic acid (NTA) moieties that can complex histidine-tagged (His-tagged) proteins selectively and reversibly. Using fluorescence microscopy, IR spectroscopy, X-ray photoelectron spectroscopy, surface plasmon resonanace, and ellipsometry, we demonstrate that His-tagged green fluorescent protein can be immobilized on NTA brushes with high stability and loading. The loading saturation reached for NTA-POEGMA is higher than that for NTA-PHEMA because of increased swelling of the former brush. Despite this higher loading capacity, NTA-POEGMA remained highly protein-resistant, which shows its potential for "clean" and specific protein immobilization. Finally, we showed that the preserved protein resistance of NTA-POEGMA brushes can be used to generate well-defined binary biofunctional patterns via a simple protocol of incubations and washes. These patterns may find applications in cell arraying and screening.

**KEYWORDS:** polymer brush • protein resistance • surface plasmon resonance • histidine tag • recombinant protein

## 1. INTRODUCTION

Stable and specific immobilization of proteins and oligonucleotides on surfaces is essential for the development of many biotechnological platforms such as DNA and proteomic microarrays (1), optical biomedical sensing (2, 3), heterogeneous enzymatic catalysis (4, 5), and biofunctional micropatterned substrates for cell arraying (6). Optimal performance for these applications requires (i) a selective and stable coupling technique, ideally reversible to allow regeneration, (ii) sufficiently high and well-controlled loading capacities (for reproducibility, ease of detection, and increased bioactivity), and (iii) protein resistance to avoid nonspecific interactions and denaturation of the biomolecules immobilized.

With respect to this latter requirement, many types of coatings have been designed to limit the adsorption of unwanted proteins on surfaces. Dextran and other polysaccharides display high immobilization loadings, although often to the detriment of lower protein resistance, and are routinely used for optical detection [e.g., via surface plasmon resonance (SPR) in Biacore commercial systems] (7, 8). Other surfaces that limit nonspecific protein adsorption include zwitterionic coatings (9, 10) and peptide self-assembled monolayers (SAMs) (11). Poly(ethylene glycol) (PEG) SAMs have shown remarkable performance, although not for long-term applications or in complex concentrated media (12, 13). Finally, polymer brushes based on PEG derivatives, such as poly(oligoethylene glycol methacrylate) (POEGMA) and poly(hydroxyethyl methacrylate) (PHEMA) (Figure 1), have shown remarkable cell and protein resistance, even after prolonged times or in the presence of complex concentrated mixtures such as a cell culture medium and undiluted sera (14−16). These exceptional performances are due to a combination of their neutral PEG chemical structure and their high thickness (compared to SAMs) and grafting density, which are made possible by the "grafting from" atom-transfer radical polymerization (ATRP) approach.

Such high protein resistance, however, seems to hinder facile and high loading functionalization of POEGMA brushes with proteins, presumably because large biomolecules do not reside in the vicinity of the coating for sufficiently long times to react. Therefore, POEGMA biofunctionalization strategies have relied on highly selective and robust couplings such as $O^6$-benzylguanine/AGT fusion proteins (17) and biotin/streptavidin (18, 19) couples. The present article reports the functionalization of POEGMA brushes with nickel nitrilotriacetic acid (Ni-NTA) ligands, which can selectively bind histidine-tagged (His-tagged) proteins while preserving their antifouling performance. We conducted a parallel study

* To whom correspondence should be addressed. E-mail: jeg45@cam.ac.uk (J.E.G.), kmr48@cam.ac.uk (M.R.).
Received for review September 24, 2009 and accepted November 12, 2009
† Department of Chemistry, University of Cambridge.
‡ Department of Biochemistry, University of Cambridge.
§ Umeå University.
DOI: 10.1021/am9006484

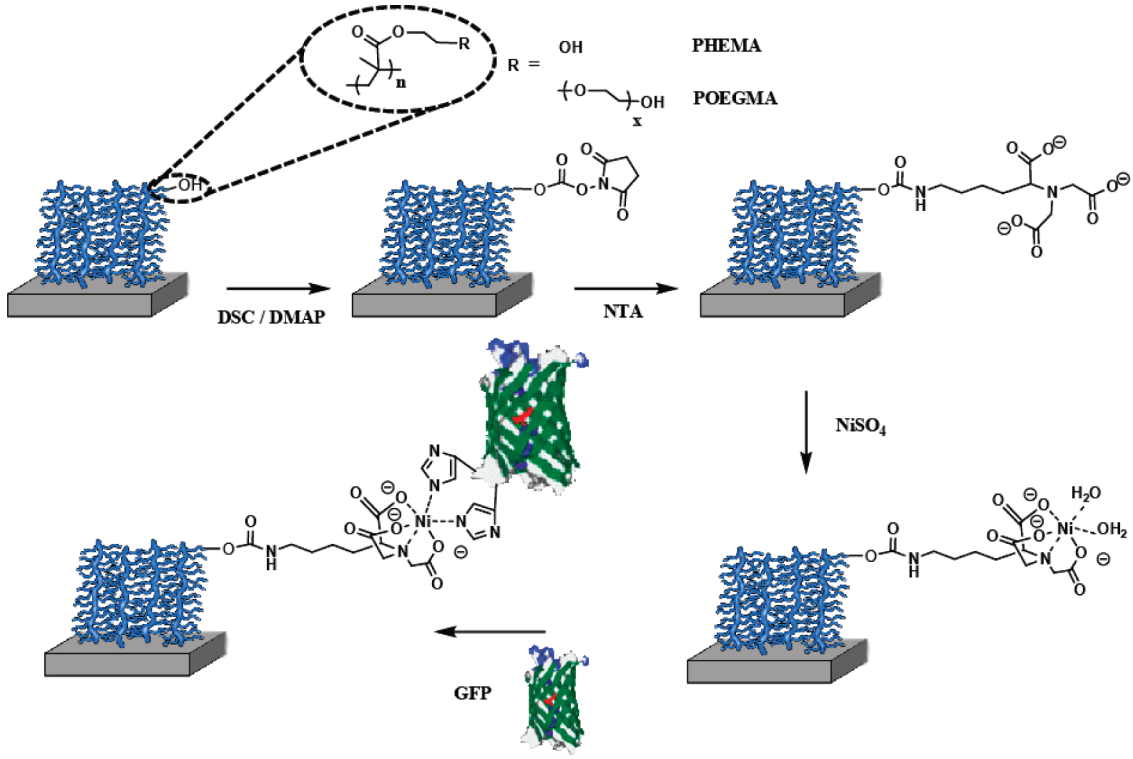


**FIGURE 1. Structure and functionalization of polymer brushes with NTA ligands, followed by His-GFP immobilization.**

with NTA-functionalized PHEMA brushes and compared the levels of His-tagged green fluorescent protein (His-GFP) immobilization and the protein resistance of the two coatings. The two major aims of this study are to demonstrate the possible selective and directed immobilization of His-tagged proteins on POEGMA brushes and the preserved nonspecific protein resistance of the resulting coatings. We then give an example of how these properties can be used to generate binary biofunctional patterns. Such micropatterns may be particularly useful for applications such as microarraying, cell arraying, and screening.

Ni-NTA chelating agents are particularly attractive because they can be switched on and off using competitive chelators such as ethylenediaminetetraacetic acid (EDTA) or imidazole. The relatively high loading that can be achieved, together with the inherent 3D architecture of the polymer brushes, ensures multiple point attachment and rebinding, a necessary requirement for stable immobilization considering the moderately high dissociation constant of Ni-NTA/His-tagged complexes (on the order of $10^{-13}$ $M^{-1}$) (20−23). In addition, immobilization of His-tagged proteins is particularly appealing because of the ubiquity of this tag in recombinant protein synthesis and purification. We use a His-tagged green fluorescent protein (His-GFP) as a proof of concept because of its extensive characterization in other systems, allowing comparisons to be made, and the additional detection method via fluorescence microscopy that it provides. Ni-NTA polymer brushes based on poly(acrylic acid) (24, 25) or PHEMA (26) have been reported in the literature. In these reports, extremely high loading levels were achieved, corresponding to up to 30 "monolayers" of protein. This is a particularly useful property for the preparation of functional membranes to be used for protein purification (26). However, a marked increase in protein denaturation and a decrease in the enzymatic activity were reported for the highest protein loadings (25). In addition, these coatings were not designed to be protein-resistant.

## 2. EXPERIMENTAL DETAILS

**2.1. Materials.** Oligo(ethylene glycol methacrylate) (OEGMA; $M_w = 360$), 2-hydroxyethyl methacrylate (HEMA), CuCl, $CuBr_2$, 2,2′-dipyridyl (bpy), disuccinimidyl carbonate (DSC), 4-(dimethylamino)pyridine (DMAP), dimethylformamide (DMF), *N*,*N*-bis(carboxymethyl)-L-lysine, methoxyethanolamine, ethylenediaminetetraacetic acid (EDTA), nickel sulfate, imidazole, bovine serum albumin (≥96%, cell culture tested grade), and phosphate-buffered saline (PBS; 150 mM) were purchased from Aldrich and used as received. ω-Mercaptoundecyl bromoisobutyrate **1** was synthesized according to the literature (27). Milli-Q water was obtained using a Synergy system from Millipore. Silicon wafers (Compart Technology Ltd.) were coated with chromium (15 nm) and gold (200 nm; Birmingham Metal) using an Edwards Auto 500 evaporator. For sample preparation, gold-coated wafers were cut into 1 $cm^2$ squares.

**2.2. Cloning, Expression, and Purification of GFP.** The gene encoding for the green fluorescent protein (GFP) was cloned into pQE-70 (Qiagen) from pGreen-TIR (28). The pQE-70 vector adds a hexahistidine tail at the C terminus of the protein sequence.

The coding sequence for GFP was amplified using a polymerase chain reaction (PCR) from pGreen-TIR using the primers 5′CCCGCATGCGAAGTAAAGGAGAAGAACTTTTC3′ (fwd SphI) and 5′CCCAGATCTTTTGTAGAGCTCATCCATGCC3′ (rev BglII). The PCR product was purified, digested with SphI and BglII (New England BioLabs), and inserted into pQE-70 digested with SphI and BglII. The resulting construct was introduced into *Escherichia coli* (Strategene XL1-Blue electroporation competent cells) by electroporation. Overnight cultures (10 mL) of transformed

cells were added to flasks containing 500 mL of Luria Broth. All bacterial cultures were prepared with 50 $\mu$g mL$^{-1}$ carbenicillin. The fresh culture was grown at 37 °C until the late exponential phase (OD $\sim$ 0.6), and 0.5 mL of 1 M isopropyl $\beta$-D-1-thiogalactopyranoside (IPTG) was added to each flask. The cells were left to overexpress the protein in the presence of IPTG for 2 h at 37 °C and were subsequently pelleted by centrifugation (20 min, 8000 rpm, 4 °C), and the resulting cell pellet was frozen (−20 °C). The cells in the cell pellet were resuspended and lysed in 25 mL of an ice-cold lysis buffer (50 mM $NaH_2PO_4$, 300 mM NaCl, 10 mM imidazole, pH 8) using three 2-min pulses of ultrasound. The sample was left to cool on ice between each 2-min pulse. The cell debris was removed by centrifuging twice for 20 min at 4000 rpm at 4 °C. The soluble protein was added to a Ni-NTA agarose column equilibrated with a lysis buffer. The column was subsequently washed overnight with approximately 50 column volumes of wash buffer (50 mM $NaH_2PO_4$, 300 mM NaCl, 20 mM imidazole, pH 8). The protein was eluted with approximately 10 mL of an elution buffer (50 mM $NaH_2PO_4$, 300 mM NaCl, 250 mM imidazole, pH 8). The eluted GFP protein was dialyzed three times against 1 L of a PBS solution (oxoid). In the last dialysis buffer, 10% glycerol was added to stabilize the protein during freezing. Subsequently, the protein was concentrated using Amicon Centricon YM-3 with a $M_w$ cutoff of 3000 Da. The concentration of protein was determined using an absorbance at 488 nm and an extinction coefficient of 56 000 M$^{-1}$ cm$^{-1}$ (29). The protein was quickly frozen in small aliquots using $N_2$(l) and stored at −80 °C until use. Sodium dodecyl sulfate−polyacrylamide gel electrophoresis of the purified protein gave a single band at 27 kDa.

**2.3. Polymer Brush Growth and Functionalization.** For growth of a 30-nm-thick POEGMA brush, a solution of $CuBr_2$ (9 mg, 40 $\mu$mol), bpy (160 mg, 1.0 mmol), and OEGMA (6.3 g, 17.5 mmol) in water (11 mL) was degassed using nitrogen bubbling for 30 min. CuCl (41 mg, 410 $\mu$mol) was added to this solution and the resulting mixture further degassed for 10 min before transfer to a flask containing the initiator-coated gold surface (immersion in a 5 mM ethanolic solution of $\omega$-mercaptoundecyl bromoisobutyrate overnight) under an inert atmosphere. The polymerization was stopped after 30 min by immersing the coated surface in Milli-Q water and subsequently washed with copious amounts of ethanol before drying in a nitrogen stream.

For growth of a 30-nm-thick PHEMA brush: similar to that for POEGMA brushes, using a solution of $CuBr_2$ (9 mg, 40 $\mu$mol), bpy (160 mg, 1.0 mmol), HEMA (6.3 g, 48.4 mmol), water (11 mL), and CuCl (41 mg, 410 $\mu$mol) and a polymerization time of 10 min.

Polymer brushes were activated with DSC by incubating in an anhydrous DMF solution containing DSC (0.1 M) and DMAP (0.1 M) under an inert atmosphere, at room temperature, overnight. After washing with copious amounts of DMF and Milli-Q water, the brushes were incubated in a *N*,*N*-bis(carboxymethyl)-L-lysine solution (5 mg mL$^{-1}$) in PBS (150 mM) at pH 8.5 overnight, at room temperature. Finally, brushes were washed with copious amounts of Milli-Q water and dried under nitrogen.

**2.4. Instrumental Analyses.** Grazing-angle Fourier transform infrared (FTIR) spectra were obtained on a Vertex 70 (Bruker) equipped with a mercury−cadmium−telluride detector and a Veemax II stage (Pike Technologies) with an angle of incidence of 80°. A number of 64 scans were acquired in a normal atmosphere for each sample. A new background was acquired before each scan to account for small changes in the atmospheric composition. Spectra were collected from brushes grown from gold surfaces.

X-ray photoelectron spectroscopy (XPS) analyses were performed using a Kratos Axis Ultra under monochromatic Al K$\alpha$ radiation (1486.6 eV). A pass energy of 160 eV and a step size of 1 eV were used for survey spectra. For high-energy resolution spectra of the regions, a pass energy of 20 eV and a step size of 0.1 eV were used. Charge-neutralizing equipment was used to compensate for sample charging, and the binding scale was referenced to the aliphatic component of C 1s spectra at 285.0 eV. The concentrations obtained (error of less than relatively ±10%) are reported as the percentage of that particular atom species (atom %) at the surface of the sample (<10 nm analysis depth) without any correction. The analysis area (0.3 × 0.7 mm), the angle of incidence, and the beam intensity were kept constant for all measurements. In addition, the samples were assumed to be homogeneous and with similar densities in the dry state, which should allow a direct correlation between the atom % of nitrogen and the SAM coverage density of the analysis area for the different brushes presently studied.

Fluorescence measurements were carried out on a Leica DMI 4000B microscope, with a CTR 6000 laser (excitation filter BP480/40, suppression filter B527/30, and dichromatic mirror 505). All images were recorded with identical settings (laser intensities and gains) at five incremental exposure times, to allow a wider intensity window to be probed. Measurements were carried out in triplicate, at three distant positions for each sample (average of nine values). Micropatterned substrates were prepared by microcontact printing of the ATRP thiol initiator **1** using a PDMS stamp, followed by brush growth and functionalization.

Surface plasmon resonance (SPR) was performed on a Biacore 3000. SPR chips (Ssens) were coated with the desired polymer brush (30 nm) and functionalized with NTA ligands prior to mounting on a substrate holder. Mounted chips were docked, primed with buffer (PBS) twice, and equilibrated at 20 $\mu$L min$^{-1}$ for 30 min or until a stable baseline was obtained. For immobilization of His-GFP, the programmed sequence was as follows: wash and equilibrate for 5 min, expose to a 200 mM EDTA solution for 10 min, expose to a 200 mM $NiSO_4$ solution for 30 min, expose to a His-GFP solution at the desired concentration (solution made with a running buffer) for 15 min, wash with PBS for 13 min, and wash with imidazole (200 mM in PBS) for 5 min. The GFP immobilization level is measured 10 min after the start of the washing procedure with PBS. For nonspecific adsorption to polymer brushes, a similar procedure was used, omitting the $NiSO_4$ treatment. The flow rate was 20 $\mu$L min$^{-1}$. Measurements were carried out in triplicate.

Ellipsometry measurements were performed with a $\alpha$-SE instrument from J. A. Woolam at 70° incidence angle. For dry samples, a simple gold substrate/cauchy film model was used and fitted between 400 and 900 nm. For wet samples, substrates were placed in an in-house-built chamber fitted with quartz windows normal to the laser beam path. The gold model and refractive index of the medium were obtained using data recorded for bare gold in the relevant medium (Milli-Q water or PBS). Measurements were carried out in triplicate. For dry ellipsometry, samples that had been exposed to His-GFP were briefly washed with Milli-Q water to avoid salt precipitation.

**2.5. Generation of Binary Patterns.** Microcontact printing of **1** followed by POEGMA growth allowed the preparation of micropatterned substrates presenting arrays of uncoated gold islands (60 $\mu$m in diameter) separated by a POEGMA background (90 $\mu$m between two gold islands). After functionalization of the resulting substrates with NTA ligands (following the procedure described above), they were sequentially incubated in solutions of EDTA (200 mM), collagen I (BD Biosciences, 5 $\mu$g mL$^{-1}$), $NiSO_4$ (200 mM), and His-GFP (13.4 $\mu$g mL$^{-1}$). Extensive PBS washes were carried out between and after these different steps, except after EDTA incubation. Substrates were then stained for collagen I using a rabbit $\alpha$ collagen I primary antibody (abcam) and a goat $\alpha$ rabbit conjugated to an Alexa Fluor 594 secondary antibody (Invitrogen) before fluorescence microscopy imaging.

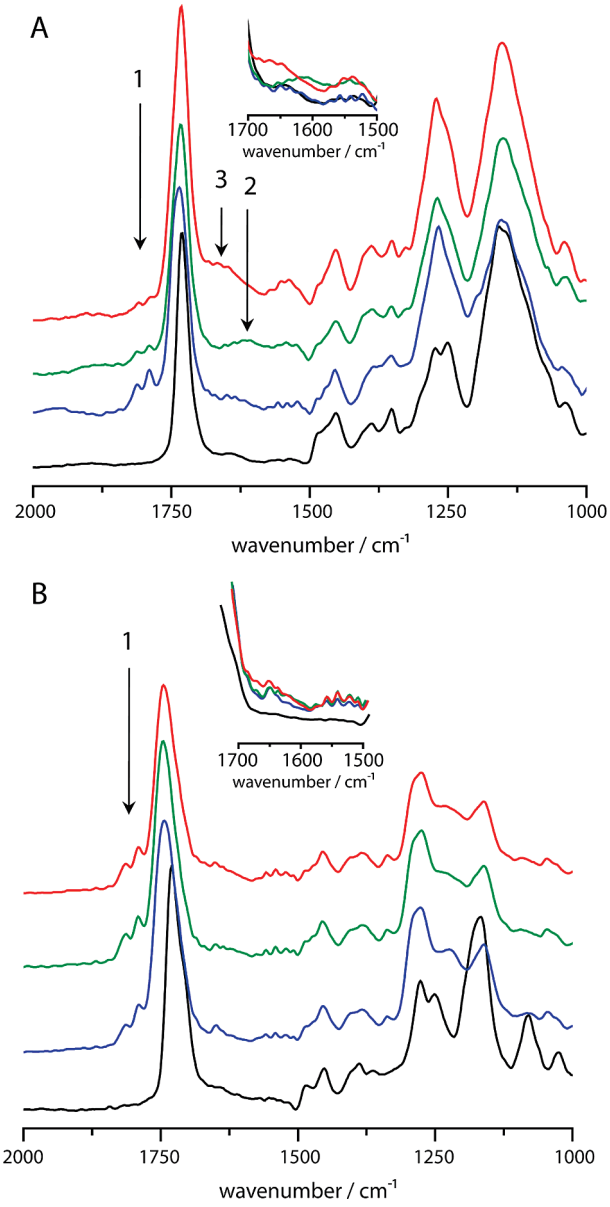


**FIGURE 2. FTIR spectra recorded for POEGMA (A) and PHEMA (B) brushes: pristine brush (black line), DSC-activated brush (blue line), Ni-NTA-functionalized brush (green line), and His-GFP-immobilized Ni-NTA brush (red line). The insets show the same spectra overlaid and magnified in the region 1500−1700 cm$^{-1}$. The arrows show specific bands that can be assigned to (1) the succinimidyl carbonate activated functions, (2) nickel carboxylates, and (3) amide I of His-GFP.**

## 3. RESULTS

Polymer brushes were prepared following standard procedures from SAMs of the ATRP initiator **1** on gold. The ATRP initiator was deposited from an ethanolic solution, undiluted with other non-ATRP active thiol. Hence, the brushes formed were prepared at the maximal grafting density.

**3.1. IR Spectroscopy.** The FTIR spectra of pristine polymer brushes display a characteristic band at 1730 cm$^{-1}$, typical of C═O stretching (Figure 2) (17). After functionalization with DSC, the presence of succinimide ester can be traced as small peaks at 1805 and 1790 cm$^{-1}$ (18). These peaks decrease in intensity after coupling to the NTA moiety, but small amounts of the activated groups can still be observed after all subsequent functionalization steps, especially for PHEMA brushes. These peaks are almost undetectable in the case of POEGMA brushes. However, further treatment of the polymer brushes with an end capper (methoxyethanolamine, 25 mg mL$^{-1}$ in PBS, pH 8.5) for 1 h did not change the immobilization or nonspecific binding results, suggesting that the remaining active groups are buried deep in the brush. Such a long lifetime for DSC-activated hydroxyl groups has been reported in the literature for PHEMA brushes (30). It is the selectivity of the carboxysuccinimidyl functions generated toward reaction with primary amines (rather than hydrolysis) that makes DSC a particularly good coupling agent for the activation of hydroxyl-terminated polymer brushes. In PHEMA, the vibrations for the succinimide ester are stronger, which indicates that more succinimide ester was formed, consistent with the smaller length of its side chains, which results in an increased terminal group density. In both polymers, the $\nu$(OH) band near 3400 cm$^{-1}$ decreases in intensity after activation because of a change of the terminal OH groups into succinimide ester groups (Figure S1 in the Supporting Information).

After coupling to the NTA moiety, a small peak originating from the carboxylate vibration appears near 1600 cm$^{-1}$ (Figure 2). The presence of this peak is clearer for POEGMA than it is for PHEMA, suggesting that a larger amount of NTA was immobilized into these former brushes. This observation, together with the lack of disappearance of the succinimide ester bands for both the POEGMA and PHEMA brushes, also indicates a relatively low level of coupling of NTA ligands. After exposure to GFP, a shoulder appears at 1640 cm$^{-1}$, which corresponds to the strongest of the protein bands, the amide I band. Similarly, this shoulder is more pronounced for POEGMA than for PHEMA brushes. The position of the amide I band is what would be expected for proteins with mainly a $\beta$-sheet secondary structure, which is the case for GFP (29).

**Table 1. Elemental Composition (atom %) for Polymer Brushes from XPS Measurements[a]**

| | Na 1s (atom %) | O sum (atom %) | N sum (atom %) | C sum (atom %) | Ni 2p (atom %) |
|---|---|---|---|---|---|
| POEGMA | | 27.7 | | 72.3 | |
| POEGMA-DSC | | 27.6 | 0.7 | 70.6 | |
| POEGMA-NTA | 0.3 | 27.2 | 1 | 71.4 | |
| POEGMA-NTA-Ni | | 27.4 | 1 | 71.4 | 0.14 |
| POEGMA-NTA-Ni-GFP | 1 | 23.3 | 6.3 | 69.4 | |
| PHEMA | | 27.8 | | 72 | 0.2 |
| PHEMA-DSC | | 29.8 | 2.9 | 67.3 | |
| PHEMA-NTA | 0.3 | 28.7 | 3.6 | 67.4 | 0.04 |
| PHEMA-NTA-Ni | | 28.3 | 3.6 | 67.5 | 0.6 |
| PHEMA-NTA-Ni-GFP | | 20.5 | 12.4 | 66.8 | 0.1 |

[a] When the sum of atom % reported does not add up to 100%, the difference is due to traces of silicon and gold detected from scratches in the film.

**3.2. XPS.** XPS spectra of PHEMA and POEGMA brushes display only oxygen and carbon signals (Table 1). After activation with succinimidyl carbonate, 0.7 and 2.9 atom % of nitrogen appear in POEGMA and PHEMA, respectively, which is consistent with the IR results showing a higher

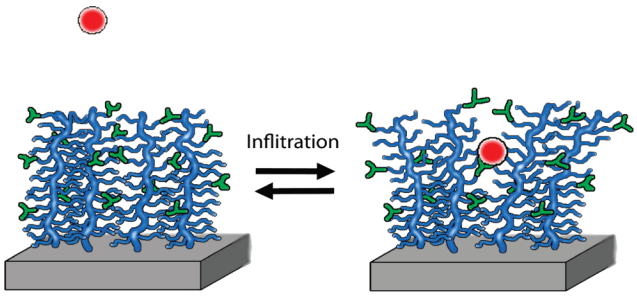


**FIGURE 3. Description of the immobilization and infiltration processes for a protein (red sphere) into a polymer brush. Ligands for specific interactions are represented in green.**

loading of activated groups on PHEMA brushes. The activation of the brushes is also evidenced in C 1s spectra with the appearance of a peak at 290.6 eV originating from carbonate groups (Figure S2 in the Supporting Information) (31).

After NTA functionalization, the nitrogen content increases slightly for both brushes, consistent with the chemical structure of the NTA moiety, which includes two nitrogen atoms (Table 1). These nitrogen contents did not change further, following immersion into $NiSO_4$ 200 mM for 1 h; however, the POEGMA and PHEMA brush surfaces displayed 0.1 and 0.6 atom % $Ni^{2+}$, respectively (Table 1). The higher nickel content of NTA-PHEMA brushes is consistent with their higher NTA density.

Important changes in XPS spectra are observed after the addition of His-GFP (Figure S2 in the Supporting Information). The nitrogen content increases to 6.3 atom % for POEGMA and 12.4 atom % for PHEMA. Thus, in contrast to the FTIR results, XPS data suggest larger protein uptake into PHEMA than POEGMA brushes. FTIR analysis probes the entire depth of the polymer film, whereas XPS only probes a superficial layer (5−10 nm). This indicates that His-GFP immobilization in PHEMA is more localized at the surface than it is in POEGMA, in which the protein infiltration seems to be increased (Figure 3). Exposure of NTA-functionalized brushes to His-GFP also leads to the appearance of an additional peak corresponding to carbon in peptide bonds at 288.0 eV in C 1s spectra. When nonfunctionalized brushes were exposed to GFP, no marked change was observed in C 1s or N signals (Figure S2 in the Supporting Information), confirming the protein resistance of these two coatings.

**3.3. Fluorescence Microscopy.** Microcontact printing was used to pattern polymer brushes onto gold surfaces (32). After NTA functionalization, His-GFP immobilization levels were determined by measurement of the fluorescence intensity on a polymer brush region and comparison to the level of the background. The fluorescence of GFP directly adsorbed onto gold is efficiently quenched, and therefore gold areas can be used as background in fluorescence measurements. In addition, protein adsorption onto gold often results in the partial denaturation of proteins, which in the case of GFP results in a loss of the photophysical properties. When POEGMA and PHEMA brushes were exposed to 13.4 $\mu$g mL$^{-1}$ His-GFP solutions (after exposure to EDTA to remove traces of metal), the level of fluorescence

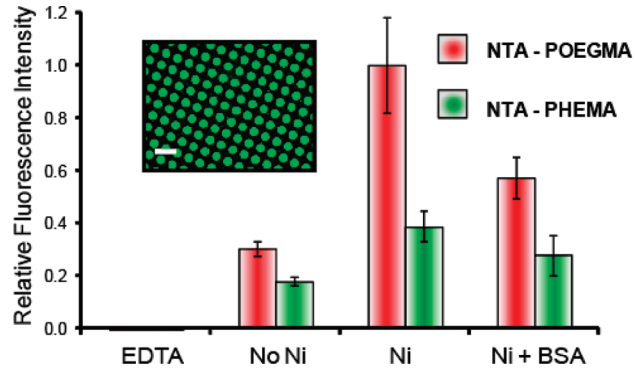


**FIGURE 4. Relative fluorescence intensities measured for NTA-functionalized polymer brushes after His-GFP immobilization (13.4 $\mu$g mL$^{-1}$). Prior to protein immobilization, brushes were treated in different conditions: i, with EDTA ("EDTA"); ii, no treatment ("No Ni"); iii, $NiSO_4$ treatment ("Ni"); iv, $NiSO_4$ treatment and immobilization carried out in a 10 mg mL$^{-1}$ BSA solution ("Ni + BSA"). The inset displays a typical fluorescence microscopy image taken for a patterned brush after simple nickel treatment and His-GFP exposure (scale bar: 100 $\mu$m).**

was below the detection threshold (polymer-brush-functionalized areas were indistinguishable from the background), consistent with the protein-resistant character of these polymer coatings. After NTA functionalization, the fluorescence level in the presence of nickel is 3−4 orders of magnitude higher than that in the absence of nickel (Figure 4). If the polymer brushes are exposed to His-GFP solutions without nickel activation, the level of fluorescence decreases by two thirds, showing that metal traces (copper used in the ATRP polymerization or metal traces present in the buffer used) can induce substantial His-tagged protein immobilization. When a high concentration of BSA (10 mg mL$^{-1}$) was mixed with the His-GFP solutions (13.4 $\mu$g mL$^{-1}$ in PBS) prepared, the fluorescence level was only reduced by a third to a half, showing the high affinity of His-GFP for the NTA brushes, despite competitive binding with BSA through weaker interactions with amino acid residues such as Cys, Glu, Asp, Arg, Lys, and His (see Figure S3 in the Supporting Information) (20). Interestingly, in all cases, the fluorescence intensity resulting from His-GFP on NTA-PHEMA brushes was half that on NTA-POEGMA. This suggests that less His-GFP is immobilized onto the former brushes and confirms the IR results that displayed stronger amide I bands when His-GFP is immobilized onto these latter brushes.

Fluorescence microscopy was also used to study the formation and quality of binary biofunctional patterns (see the Experimental Section for a detailed preparation method). Collagen I, an extracellular matrix molecule useful for promoting cell adhesion, was deposited on gold islands surrounded by a NTA-POEGMA background. Subsequent nickel incubation and His-GFP immobilization resulted in binary biofunctional patterns. In order to visualize the distribution and amounts of collagen immobilized on the substrates, staining using specific antibodies was carried out after His-GFP immobilization. The pictures taken (Figure 5) clearly demonstrate that collagen I remains localized on unprotected gold islands, whereas His-GFP is localized on the NTA-POEGMA background.

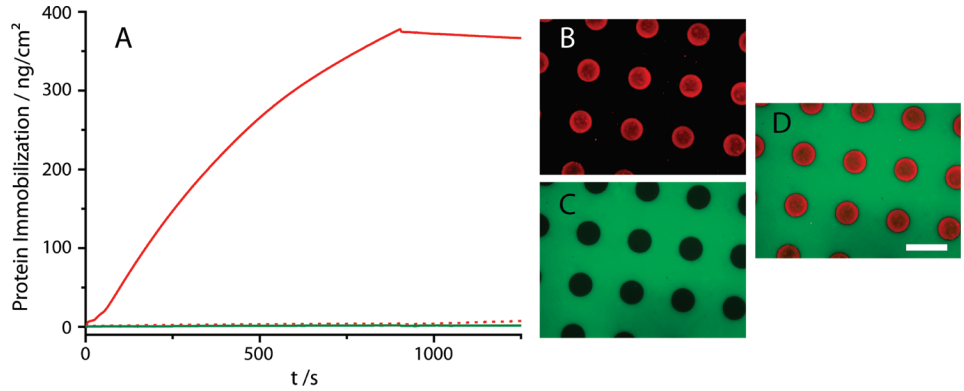


**FIGURE 5. Well-defined binary biofunctionalized patterns. (A) SPR traces recorded for NTA-POEGMA during exposure to collagen (green curve, 5 $\mu$g mL$^{-1}$ collagen I after EDTA incubation) and during exposure to His-GFP (13.4 $\mu$g mL$^{-1}$) with (solid red curve) and without nickel treatment (dotted red curve, after EDTA incubation). Images on the right display typical examples of binary patterns (detailed procedure described in the Experimental Section): (B) collagen I; (C) His-GFP; (D) merge. Scale bar: 100 $\mu$m.**

**3.4. SPR.** We examined the immobilization of His-GFP on NTA brushes in a more quantitative way using SPR. First, we carried out experiments after activation with nickel. Figure 6A displays typical examples of SPR traces. At low-to-moderate concentrations, the amount of protein immobilized increases steadily upon exposure to His-GFP solutions (step 1). Upon washing of the surface with PBS (step 2), the signal remains remarkably stable, provided that the saturation protein density has not been reached (as in the case of SPR traces in Figure 6A, except for the red one). Exposure to an imidazole solution (step 3, 200 mM in PBS) displaces the Ni-NTA/His-GFP complex, which releases most of the protein immobilized on the brush. At higher protein concentrations, when a maximum loading capacity is reached, some protein is washed off during step 2 (Figure 6A), which indicates that the complex is less stable near saturation levels. This is consistent with observations made on NTA-based SAMs and the importance of rebinding events for stabilizing the complexes formed (20, 22, 33).

Figure 6B presents the evolution of His-GFP immobilization with the protein concentration for NTA-PHEMA and NTA-POEGMA brushes. For both brushes, loading saturation is reached at around 5−10 $\mu$g mL$^{-1}$ of protein. The saturation level is near 600 ng cm$^{-2}$ for NTA-POEGMA, whereas it is only 300 ng cm$^{-2}$ for NTA-PHEMA, which is consistent with FTIR and fluorescence microscopy results but not XPS data (quantitative information can be extrapolated from SPR data, using as an approximation 1 ng cm$^{-2}$ for 10 RU (34); no further calibration of our instrument was performed). This observation further suggests a superficial immobilization of His-GFP in the case of NTA-PHEMA and some protein infiltration in the case of NTA-POEGMA. In addition, the initial rate of protein immobilization (slope of the SPR trace, just after the start of exposure to His-GFP solutions) is faster in the case of NTA-PHEMA than it is for NTA-POEGMA, at identical protein concentrations: it is 68 ± 5 and 24 ± 3 ng cm$^{-2}$ s$^{-1}$ for NTA-PHEMA and NTA-POEGMA brushes, respectively, for a 13.4 $\mu$g mL$^{-1}$ His-GFP concentration. This is consistent with the occurrence of protein infiltration, a slower process than protein diffusion in solution, in NTA-POEGMA brushes (Figure 3).

Finally, in order to test the specificity of the His tag for the Ni-NTA complex, SPR experiments were carried out after exposure of the brushes to EDTA solutions, in order to remove metal ion traces. This provides an indication of the specificity of His-tagged proteins for the two NTA-functionalized brushes. As can be observed in Figures 6C and S4 in the Supporting Information, higher immobilization levels were measured in the case of EDTA-treated NTA-PHEMA than NTA-POEGMA. This is consistent with the high performance of POEGMA-based coatings in terms of protein resistance (15, 17). The ratio of the His-GFP immobilization levels in the presence and absence of nickel is 24 for NTA-POEGMA, whereas it is only 3.2 for NTA-PHEMA. This reflects both the higher protein loading of POEGMA brushes and their better protein resistance. In addition, when the two NTA-functionalized brushes were exposed to a solution of different proteins (without His tags), after EDTA treatment, the level of nonspecific binding was consistently higher for PHEMA brushes (Figure 6C), further demonstrating the better performance of NTA-POEGMA as a selective protein-resistant coating.

**3.5. Ellipsometry.** The swelling of POEGMA and PHEMA brushes in different conditions was probed by dry and wet ellipsometry in order to better understand the processes governing protein immobilization in these brushes. The swelling of POEGMA brushes (with or without NTA ligands) was always higher than that of PHEMA brushes, in both Milli-Q water and PBS (Figure 7). This was also reflected in the lower refractive indexes for POEGMA brushes and therefore their higher water contents. In addition, the swelling of both brushes was higher in PBS than in Milli-Q water (except for NTA-PHEMA, which remained unchanged), in contrast with polyelectrolyte brushes, which typically collapse at high salt concentrations (35). Strikingly, NTA-PHEMA brushes essentially remain collapsed (20 % swelling versus 40−70 % for other brushes) in both Milli-Q water and PBS. This observation is mirrored by their higher refractive index and therefore lower water content. The swelling measured on Ni-NTA brushes were virtually identical with those measured on NTA brushes before exposure to a solution of $NiSO_4$. The lower swelling of NTA-PHEMA brushes

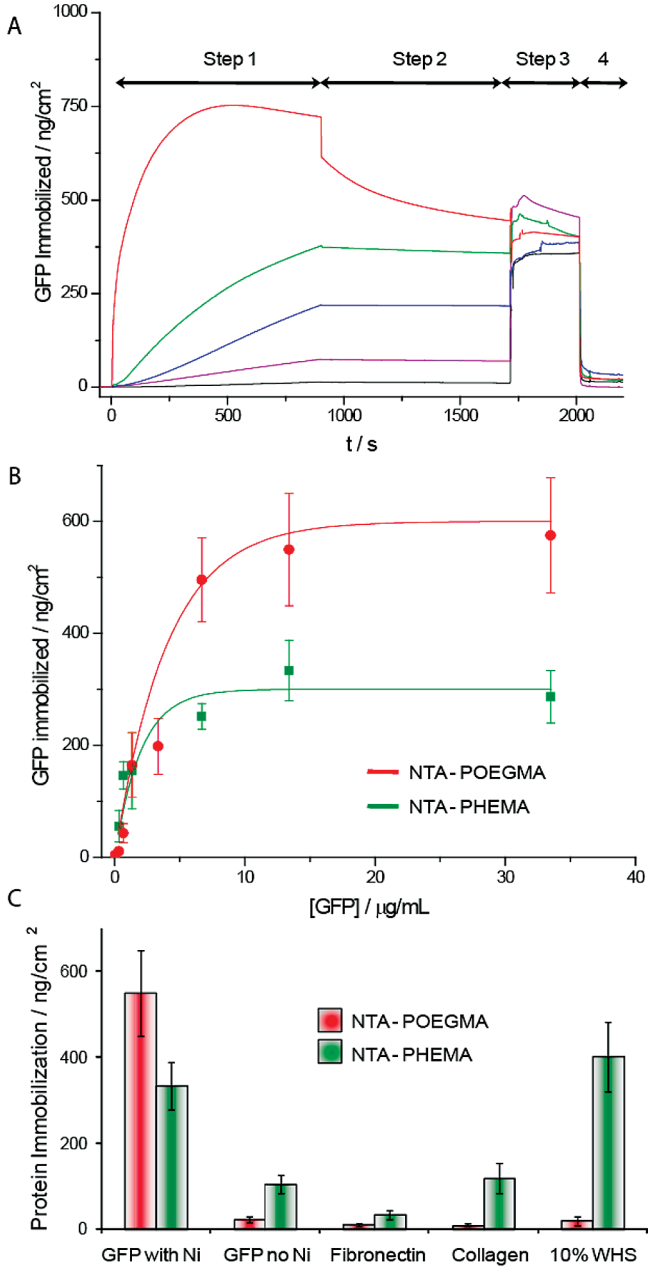


**FIGURE 6. His-GFP immobilization followed by SPR. (A) Typical SPR traces recorded for NTA-functionalized brushes (here NTA-POEGMA) after nickel activation. Step 1: exposure to a His-GFP solution in a running buffer (PBS). Step 2: exposure to a running buffer. Step 3: exposure to an imidazole solution (200 mM PBS). Step 4: exposure to a running buffer. His-GFP concentrations were 13.4 $\mu$g mL$^{-1}$ (red), 6.7 $\mu$g mL$^{-1}$ (green), 1.34 $\mu$g mL$^{-1}$ (blue), 335 ng mL$^{-1}$ (purple), and 67 ng mL$^{-1}$ (black). (B) Levels of His-GFP immobilization after 10 min of washing with a running buffer for NTA-POEGMA (red) and NTA-PHEMA (green). The solid lines are guides for the eye. (C) Levels of protein immobilization after 10 min of washing with a running buffer for NTA-POEGMA (red) and NTA-PHEMA (green). NTA brushes were treated with nickel ("GFP with Ni") or EDTA (the rest of the data) before exposure to protein solutions (concentrations: His-GFP, 13.4 $\mu$g mL$^{-1}$; fibronectin, 5 $\mu$g mL$^{-1}$; collagen, 5 $\mu$g mL$^{-1}$; WHS, whole horse serum diluted to 10% in PBS).**

may be due to higher levels of brush cross-linking (for example, via the formation of carbonate bonds), a process that may occur during brush activation and functionalization, given the higher activated group density in this brush.

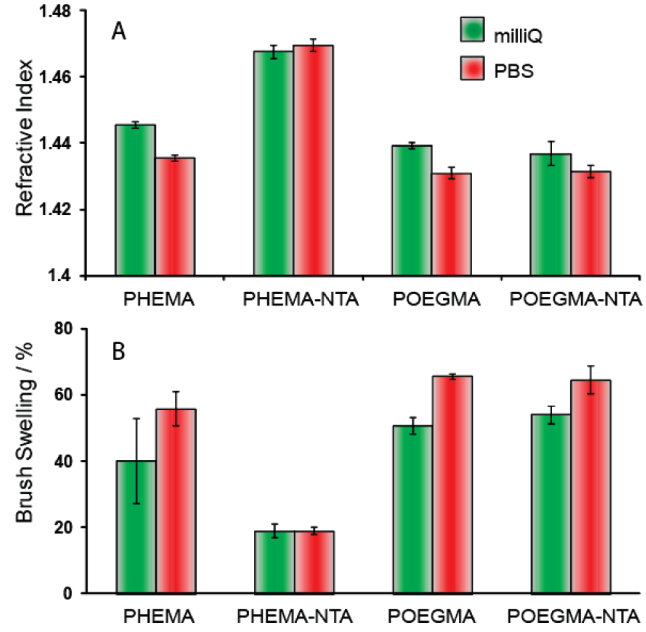


**FIGURE 7. Refractive index (A) and swelling (thickness increase relative to the dry thickness) changes (B) measured by ellipsometry for pristine and NTA-functionalized brushes in Milli-Q water (green) and PBS (red).**

**Table 2. Increase in the Ellipsometric Thickness Measured after Exposure to His-GFP (13.4 $\mu$g mL$^{-1}$)**

| | PBS ( nm)[a] | dry (nm)[b] |
|---|---|---|
| PHEMA | 1.5 ± 1.8 | −0.3 ± 0.3 |
| PHEMA-NTA | 1.7 ± 0.4 | 0.3 ± 0.3 |
| PHEMA-NTA-Ni | 3.7 ± 1.5 | 3.0 ± 0.8 |
| POEGMA | 0.1 ± 0.2 | 0.1 ± 0.2 |
| POEGMA-NTA | 0.4 ± 1.4 | −0.3 ± 0.8 |
| POEGMA-NTA-Ni | 4.6 ± 0.7 | 2.5 ± 0.4 |

[a] The surfaces were exposed to His-GFP (13.4 mg mL$^{-1}$) for 15 min, washed with PBS, and finally immersed in PBS for measurements. [b] After wet ellipsometry measurement, the samples were briefly washed with Milli-Q water and dried in a nitrogen stream before dry measurement.

Such a low propensity to swell does not favor protein infiltration and may explain why His-GFP saturation loadings are higher for NTA-POEGMA brushes (as determined by SPR).

Finally, changes in the ellipsometric thickness upon His-GFP immobilization were measured both in PBS and after drying (Table 2). For nonfunctionalized and NTA-functionalized brushes treated with EDTA, little change in the thickness is measured. In PBS, the thickness of PHEMA brushes seems to increase slightly, supporting their lower protein resistance, but no significant change in the dry thickness can be observed. This difference between the wet and dry thickness may be due to the final washing step, required to avoid salt crystallization on the surface, which significantly affects ellipsometry measurements. When NTA-functionalized brushes are exposed to His-GFP, their thicknesses increase by 2−5 nm, which corresponds to a monolayer of GFP (which is approximately a cylinder of 2 nm diameter by 4 nm height (36)). Given the relatively large standard

errors measured, the immobilization levels measured by ellipsometry for both brushes are equivalent.

## 4. DISCUSSION

**4.1. Stable Immobilization of Hexahistadine-Tagged Proteins.** Fluorescence and SPR measurements clearly demonstrate that high levels of His-GFP immobilization are achieved on NTA-functionalized PHEMA and POEGMA brushes. Nearly 600 and 300 ng $cm^{-2}$ of His-GFP can be immobilized on POEGMA and PHEMA, respectively (Figure 6A). The surface loadings calculated for densely packed GFP monolayers are 440 and 780 ng $cm^{-2}$, for side-on and base-on adsorption (36). However, it is unlikely that GFP would adopt such a highly ordered packing, which is reflected by the lower protein densities reported in the literature for adsorption of His-GFP on NTA-based SAMs: Choi and co-workers reported 120 ng $cm^{-2}$ for a thiol-based NTA SAM (37), whereas Zürcher and co-workers obtained 30−100 ng $cm^{-2}$ for adsorbed copolymer layers (38). The lower immobilization level reported in this latter case may be due to lower NTA ligand densities. Other His-tagged proteins and antibodies were immobilized on NTA SAMs at similar loadings (100−450 ng $cm^{-2}$), although these levels should be compared with care, given the large range of protein sizes used (22, 33, 39). Therefore, our results demonstrate that, despite the relatively low NTA functionalization level (especially for POEGMA), high His-tagged protein immobilization loadings can be achieved even at subnanomolar concentrations. This behavior is a direct consequence of the 3D architecture of polymer brushes, which contrasts with that of SAMs: polymer brushes swell in good solvents, which facilitates the infiltration of small objects, such as nanoparticles or proteins (40). Hence, substantially higher protein loading levels may be achieved.

In addition, the Ni-NTA/His-tagged complex typically requires high NTA densities and low protein loading levels in order to remain stable (20−22). To improve the stability of such a complex on surfaces, bis- and tri-NTA chelators have recently been designed. Thanks to the local high density of the NTA ligand that SAMs of these molecules display, higher protein loadings, together with improved complex stability, were achieved (20, 21). Another strategy is to use decahistidine tags (20). The excellent stability of the complexes formed in POEGMA and PHEMA brushes, even at relatively high protein loadings (up to 400 ng $cm^{-2}$; Figure 6A), indicates that the 3D architecture of the polymer brushes provides high local NTA densities and favors protein rebinding events. In addition, the partial entanglement that results from protein infiltration may kinetically favor protein rebinding and help to stabilize the complexes formed. However, at the highest protein concentrations (above 5 $\mu$g $mL^{-1}$), when the level of loading reaches saturation, the stability of the complex is lower because the density of "free" NTA ligands is too low for rebinding to be significant (as is the case in the red curve in Figure 6A). Similar phenomena were reported for NTA-based SAMs (20, 22, 33).

Finally, the immobilization levels that are reported for other NTA-functionalized polymer brushes, based on poly(acrylic acid) or PHEMA, are significantly higher than those reported in the present study (24−26). The formation of up to 30 protein monolayers was observed. These observations may be due to the significantly larger swelling reported in these studies [poly(acrylic acid) is known to swell considerably in water, and the PHEMA brushes prepared may have lower grafting densities, due to differences in the initiator layer formation] but also due to differences in the methods used to determine these loadings. However, reports have shown that, at high loading levels, significant protein denaturation (and subsequent loss of enzymatic activity in the case of enzymes) was measured. Low protein denaturation in the case of the NTA-POEGMA and NTA-PHEMA presently discussed is evidenced by the reversibility of the immobilization (Figure 6A) because denaturation is usually associated with irreversible adsorption to surfaces, as well as FTIR and fluorescence microscopy measurements (GFP fluorescence is quenched when denatured).

**4.2. GFP Infiltration in Polymer Brushes.** The levels of loading saturation measured for the immobilization of His-GFP in NTA-POEGMA brushes are twice those measured for NTA-PHEMA brushes, as determined by SPR and fluorescence microscopy (Figures 4 and 6). Interestingly, XPS measurements indicate the opposite (Table 1): the level of nitrogen measured in NTA-PHEMA brushes exposed to a 13.4 $\mu$g $mL^{-1}$ solution of His-GFP (followed by washing with PBS for 1 h) is twice that measured for NTA-POEGMA brushes. XPS is a technique that probes only the superficial layer of a material, typically (and in the measurement conditions used in the present study) the top first 5−10 nm. Therefore, our results indicate that GFP is infiltrating NTA-POEGMA brushes much deeper than it does for NTA-PHEMA. Indeed, a superficial immobilization of protein will result in a more intense XPS peak than a more homogeneous distribution throughout a film, at identical total loadings.

In order to confirm that differences in protein infiltration are indeed responsible for the XPS measurements obtained, we conducted a series of ellipsometry measurements with blank POEGMA and PHEMA brushes and their corresponding NTA-functionalized homologues. The swelling level (compared to the dry thickness) of POEGMA brushes is higher than that measured for PHEMA brushes, and it is higher in 150 mM PBS than in Milli-Q water. Most striking is the low swelling of NTA-PHEMA (which barely changes when going from Milli-Q water to 150 mM PBS; Figure 7). These observations are mirrored by changes in the refractive indexes of the brushes, showing much lower water contents in NTA-PHEMA brushes than for the three other types of surfaces tested. Therefore, ellipsometry results indicate that NTA-PHEMA brushes remain almost entirely collapsed in Milli-Q and 150 mM PBS. Such behavior restricts the infiltration of objects and is consistent with the observation of superficial protein immobilization in NTA-PHEMA brushes.

In addition, the rate of immobilization measured by SPR is higher for PHEMA (68 ± 5 ng $cm^{-2}$ $s^{-1}$) than it is for

POEGMA ($24 \pm 3$ ng cm$^{-2}$ s$^{-1}$) at identical protein concentrations (13.4 $\mu$g mL$^{-1}$). This is consistent with a deeper infiltration of His-GFP in NTA-POEGMA brushes: the kinetics of diffusion and infiltration through polymer brushes is slower than simple diffusion to the surface of the brush, which translates into slower immobilization kinetics.

**4.3. NTA-POEGMA Brushes Retain Their Protein Resistance and Allow Binary Biofunctional Patterning.** POEGMA brushes range amoung the most protein-resistant coatings available. This is presumably due to a combination of the physicochemical properties of their PEG side chains, high surface density, and thickness. Some proteins, such as fibronectin and collagen, do stick to these brushes, although to low levels (below 20 ng cm$^{-2}$, as determined by SPR, for a high-concentration protein solution of 1 mg mL$^{-1}$; results not shown). Interestingly, some proteins present in sera, especially whole horse serum, stick to these brushes. Nevertheless, the resulting nonspecifically bound protein density is much lower for POEGMA than it is for PHEMA ($88 \pm 12$ and $164 \pm 7$ ng cm$^{-2}$, respectively, from 100% whole horse serum, as determined by SPR). The protein resistance of NTA-functionalized polymer brushes follows a similar trend, although the nonspecific binding is higher than that of nonfunctionalized brushes: NTA-PHEMA brushes display higher nonspecific binding levels than NTA-POEGMA brushes, as determined by SPR in the absence of transition metals (Figure 6C). Hence, the ratio of protein immobilization for NTA-POEGMA with and in the absence of nickel ions is 24, whereas it is only 3.2 for NTA-PHEMA. This clearly demonstrates the potential of POEGMA brushes for "clean", specific, and high loading of His-tagged proteins in order to generate biofunctional surfaces.

One interesting feature of polymer brushes is that they are amenable to multicomponent patterning, which allows generation of substrates presenting several well-defined overlaying patterns with controlled surface chemistry (41). In order to demonstrate the feasibility of using our NTA-brush platform for the preparation of binary biofunctional patterns, we used microcontact printing followed by POEGMA growth to generate arrays of gold islands surrounded by a NTA-POEGMA background. The retained protein resistance of NTA-POEGMA, even upon exposure to relatively "sticky" proteins such as collagen and fibronectin, was then used to selectively deposit collagen I onto the gold island, without functionalization of the NTA-POEGMA background. Such deposition can be performed at relatively low protein concentrations (5−20 $\mu$g mL$^{-1}$), at which adhesion to NTA-POEGMA almost falls within the noise level, as evidenced by SPR (Figure 5). Deposition of His-GFP can then simply be carried out by activation of NTA-POEGMA with nickel and incubation in a His-GFP solution. Fluorescence microscopy confirmed the excellent control over the localization of both molecules (collagen and GFP; see Figure 5). Such a tool may be useful for cell patterning and screening studies, for example, in which the effect of immobilization of a His-tagged protein on the behavior of single cells (but also clusters of cells) adhering to collagen-coated islands would be studied.

## 5. CONCLUSIONS

The high specificity of NTA-POEGMA brushes, together with their preserved protein resistance and substantial protein loading, is a particularly important feature for the study of protein−protein interactions (e.g., antibody−antigen and enzyme−substrate) in a controlled fashion. These brush-coated surfaces limit peripheral nonspecific interactions with the underlying substrate and constitute an ideal platform for proteomic analysis. In addition, the high loading capacity and stability are clear advantages for generating catalytically active surfaces when enzymes are immobilized. Because of the directional and specific coupling provided by His-tagged/Ni-NTA complexes, combined with their unique hydrophilic microenvironment, the activity of enzymes may be preserved longer. Finally, the ease with which polymer brushes may be micropatterned on a variety of substrates makes NTA-brushes powerful tools for the generation of biofunctional patterns for cell studies. Such technology may be particularly useful for the study of cell response to specific cues in a controlled and automated fashion.

**Acknowledgment.** We thank Ron Oren for help with ellipsometry measurements. We thank Prof. F. Watt for allowing access to the Leica microscope for fluorescence measurements. J.E.G. thanks the Cambridge Cancer Centre for a pilot research award. M.W. is thankful for funding from the BBSRC (Grant BB/C500252/1).

**Supporting Information Available:** FTIR spectra in the 2500−4000 cm$^{-1}$ range, XPS spectra, fluorescence microscopy results at different His-GFP concentrations (in the presence of BSA), and typical SPR traces recorded for NTA-PHEMA and NTA-POEGMA with and without Ni activation. This material is available free of charge via the Internet at http://pubs.acs.org.

### REFERENCES AND NOTES

(1) Wark, A. W.; Lee, H. J.; Corn, R. M. *Angew. Chem., Int. Ed.* **2008**, *47*, 644–652.
(2) Homola, J. *Chem. Rev.* **2008**, *108*, 462–493.
(3) Anker, J. N.; Hall, W. P.; Lyandres, O.; Shah, N. C.; Zhao, J.; van Duyne, R. P. *Nat. Mater.* **2008**, *7*, 442–453.
(4) Reetz, M. T.; Zonta, A.; Simpelkamp, J. *Angew. Chem., Int. Ed.* **1995**, *34*, 301–303.
(5) Sheldon, R. A. *Adv. Synth. Catal.* **2007**, *349*, 1289–1307.
(6) Kane, R. S.; Takayama, S.; Ostuni, E.; Ingber, D. E.; Whitesides, G. M. *Biomaterials* **1999**, *20*, 2363–2376.
(7) O'Shannessy, D. J.; Burke, M. B.; Peck, K. *Anal. Biochem.* **1992**, *205*, 132–136.
(8) Yang, C.-Y.; Brooks, E.; Li, Y.; Denny, P.; Ho, C.-M.; Qi, F.; Shi, W.; Wolinsky, L.; Wu, B.; Wong, D. T. W.; Montemagno, C. D. *Lab Chip* **2005**, *5*, 1017–1023.
(9) Ladd, J.; Zhang, Z.; Chen, S.; Hower, J. C.; Jiang, S. *Biomacromolecules* **2008**, *9*, 1357–1361.
(10) Vaisocherova, H.; Yang, W.; Zhang, Z.; Cao, Z.; Cheng, G.; Piliarik, M.; Homola, J.; Jiang, S. *Anal. Chem.* **2008**, *80*, 7894–7901.
(11) Chelmowski, R.; Koster, S. D.; Kerstan, A.; Prekelt, A.; Grunwald, C.; Winkler, T.; Metzler-Nolte, N.; Terfort, A.; Woll, C. *J. Am. Chem. Soc.* **2008**, *130*, 14952–14953.
(12) Prime, K. L.; Whitesides, G. M. *J. Am. Chem. Soc.* **1993**, *115*, 10714–10721.

(13) Cheng, G.; Zhang, Z.; Chen, S.; Bryers, J.; Jiang, S. *Biomaterials* **2007**, *28*, 4192–4199.
(14) Brown, A. A.; Khan, N. S.; Steinbock, L.; Huck, W. T. S. *Eur. Polym. J.* **2005**, *41*, 1757–1765.
(15) Fan, X.; Lin, L.; Messersmith, P. B. *Biomacromolecules* **2006**, *7*, 2443–2448.
(16) Ma, H.; Li, D.; Sheng, X.; Zhao, B.; Chilkoti, A. *Langmuir* **2006**, *22*, 3751–3756.
(17) Tugulu, S.; Arnold, A.; Sielaff, I.; Johnsson, K.; Klok, H.-A. *Biomacromolecules* **2005**, *6*, 1602–1607.
(18) Lee, B. S.; Chi, Y. S.; Lee, K.-B.; Kim, Y.-G.; Choi, I. S. *Biomacromolecules* **2007**, *8*, 3922–3929.
(19) Trmcic-Cvitas, J.; Hasan, E.; Ramstedt, M.; Li, X.; Cooper, M. A.; Abell, C.; Huck, W. T. S.; Gautrot, J. E. *Biomacromolecules* **2009**, *10*, 2885–2894.
(20) Lata, S.; Piehler, J. *Anal. Chem.* **2005**, *77*, 1096–1105.
(21) Valiokas, R.; Klenkar, G.; Tinazli, A.; Reichel, A.; Tampe, R.; Piehler, J.; Liedberg, B. *Langmuir* **2008**, *24*, 4959–4967.
(22) Nieba, L.; Nieba-Axmann, S. E.; Persson, A.; Hamalainen, M.; Edebratt, F.; Hansson, A.; Lidholm, J.; Magnusson, K.; Karlsson, A. F.; Pluckthun, A. *Anal. Biochem.* **1997**, *252*, 217–228.
(23) Schmitt, J.; Hess, H.; Stunnenberg, H. G. *Mol. Biol. Rep.* **1993**, *18*, 223–230.
(24) Dai, J.; Bao, Z.; Sun, L.; Hong, S. U.; Baker, G. L.; Bruening, M. L. *Langmuir* **2006**, *22*, 4274–4281.
(25) Cullen, S. P.; Liu, X.; Mandel, I. C.; Himpsel, F. J.; Gopalan, P. *Langmuir* **2008**, *24*, 913–920.
(26) Jain, P.; Sun, L.; Dai, J.; Baker, G. L.; Bruening, M. L. *Biomacromolecules* **2007**, *8*, 3102–3107.
(27) Jones, D. M.; Brown, A. A.; Huck, W. T. S. *Langmuir* **2002**, *18*, 1265–1269.
(28) Miller, W. G.; Lindow, S. E. *Gene* **1997**, *191*, 149–153.
(29) Tsien, R. Y. *Annu. Rev. Biochem.* **1998**, *67*, 509–544.
(30) Diamanti, S.; Arifuzzaman, S.; Elsen, A.; Genzer, J.; Vaia, R. A. *Polymer* **2008**, *49*, 3770–3779.
(31) Beamson, G.; Briggs, D. *High resolution XPS of organic polymers. The Scienta ESCA300 database*; John Wiley and Sons: Chichester, U.K., 1992.
(32) Jones, D. M.; Smith, J. R.; Huck, W. T. S.; Alexander, C. *Adv. Mater.* **2002**, *14*, 1130–1134.
(33) Kroger, D.; Liley, M.; Schiweck, W.; Skerra, A.; Vogel, H. *Biosens. Bioelectron.* **1999**, *14*, 155–161.
(34) Liedberg, B.; Lundstrom, I.; Stenberg, E. *Sens. Actuators, B* **1993**, *11*, 63–72.
(35) Zhou, F.; Huck, W. T. S. *Phys. Chem. Chem. Phys.* **2006**, *8*, 3815–3823.
(36) Zimmer, M. *Chem. Rev.* **2002**, *102*, 759–781.
(37) Lee, J. K.; Kim, Y.-G.; Chi, Y. S.; Yun, W. S.; Choi, I. S. *J. Phys. Chem. B* **2004**, *108*, 7665–7673.
(38) Zhen, G.; Falconnet, D.; Kuennemann, E.; Voros, J.; Spencer, N. D.; Textor, M.; Zürcher, S. *Adv. Funct. Mater.* **2006**, *16*, 243–251.
(39) Sigal, G. B.; Bamdad, C.; Barberis, A.; Strominger, J.; Whitesides, G. M. *Anal. Chem.* **1996**, *68*, 490–497.
(40) Yoshikawa, C.; Goto, A.; Tsujii, Y.; Fukuda, T.; Kimura, T.; Yamamoto, K.; Kishida, A. *Macromolecules* **2006**, *39*, 2284–2290.
(41) Zhou, F.; Zheng, Z.; Yu, B.; Liu, W.; Huck, W. T. S. *J. Am. Chem. Soc.* **2006**, *128*, 16253–16258.

AM9006484